RSC Advances

ROYAL SOCIETY OF CHEMISTRY

www.rsc.org/advances

Journal Name

RSCPublishing

ARTICLE

p-Aminobenzoic Acid Polymorphs Under High Pressures

Cite this: DOI: 10.1039/x0xx00000x

Tingting Yan[a], Kai Wang[a,*], Defang Duan[a], Xiao Tan[a], Bingbing Liu[a], and Bo Zou[a,*]

Received 00th January 2012,
Accepted 00th January 2012

DOI: 10.1039/x0xx00000x

www.rsc.org/

The effect of high pressure on two forms (α, β) of *p*-aminobenzoic acids (PABA) is studied in a diamond anvil cell using *in situ* Raman spectroscopy. Previous research showed that α-PABA undergoes a phase transition, and β-PABA is transformed to α-PABA at high temperatures. In the present study, we investigate whether a new polymorph or a transformation between the two polymorphs occurs upon the application of pressure. Experimental results reveal that the two forms remain stable up to ~13 GPa. *Ab initio* calculations are performed to account for the changes in unit cell parameters, molecular arrangements, and hydrogen bonds. Polymerization is observed in type *B* molecules of α-PABA through the calculated geometric parameters of hydrogen bonds. Based on a systematic comparison of the subtle structural changes, anisotropic characteristic, and various interactions of the two polymorphs, we propose that the stability of α-form crystals is associated with the special dimer structure. The stability of the β-form is attributed to hydrogen-bonded networks with four-membered ring construction.

Introduction

Polymorphism, a condition in which more than one crystalline form exists in a compound, is a significant phenomenon.[1] This phenomenon is frequently observed in organic materials.[2-6] In polymorphs, each form has the same chemical composition but different conformations or molecular arrangements. Solid forms of the same compound exhibit different physicochemical properties, such as solubility, density, conductivity, and tensile strength.[7] These properties are extremely important, and industries have a huge stake in storing, handling, and processing these forms. Especially in pharmaceutical industries, drug products undergo various manufacturing processes before reaching their commercially available form. The form of a pharmaceutically active compound can determine its activity and toxicity.[8-11] Knowledge of the structural stability of polymorphs is thus fundamental and significant for physics, chemistry, and pharmaceutics.

As the most pervasive and important intermolecular interactions, hydrogen bonding plays an important role in polymorphism due to its directionality, reversibility, and saturability. High pressure has been successfully used to investigate the hydrogen-bonded polymorphic systems, as the application of pressure can provide precise tuning of intermolecular distances.[12-15] Therefore, hydrogen-bonded polymorphs under high pressures have recently been the subject of extensive research and exhibited rich phenomena.[16-21] The orthorhombic and monoclinic polymorphs of L-cysteine are differently affected under identical compression/decompression conditions, implying the kinetic control of pressure-induced phase transitions in crystalline amino acids.[22] High-pressure recrystallization of piracetam, a drug compound, generates a new polymorph; hydrogen bonds and crystal structure are thus relevant.[23] Studies of hydrogen-bonded polymorphs utilizing high-pressure technique can explore the structural stability of polymorphs and elucidate more on the nature of hydrogen bonds.

The model compound in this study is *p*-aminobenzoic acid ($C_7H_7NO_2$, PABA), an organic compound that possesses different functional groups similar to numerous drug molecules. PABA is primarily used in pharmaceuticals; this compound functions as an important active ingredient in manufacturing dyes, sunscreens, perfumes, and feedstock additives. The polymorphs of PABA have gained considerable interest among scientists.[24,25] The transformation of two PABA polymorphs (α- and β-forms) has been extensively investigated at ambient pressure. Jarchow and Banerjee[26-27] confirmed the phase transition of α-form crystals at about 32 °C by analysing the rotation of the NH_2 group about the C–N bond via NMR. Gracin[28] reported the existence of a transformation temperature between the two forms at approximately 25 °C upon crystallization from solvents; β-PABA is thermodynamically stable below this temperature. Yang et al. revealed the transformation of β-form to the α-form upon heating to 96 °C.[29] Whether a new polymorph or a transformation between the two polymorphs occurs upon the application of pressure remains unknown.

In the present study, *in situ* Raman spectroscopy is conducted to investigate the high-pressure behaviours of the (α, β) forms of PABA. The procedure is a valuable and accurate technique to examine and analyse the modifications in molecular configurations under high pressures. We perform computations to determine the changes in unit cell parameters, molecular arrangements, and hydrogen bonds. We analyse the mechanism of the structural stability, as well as cooperative

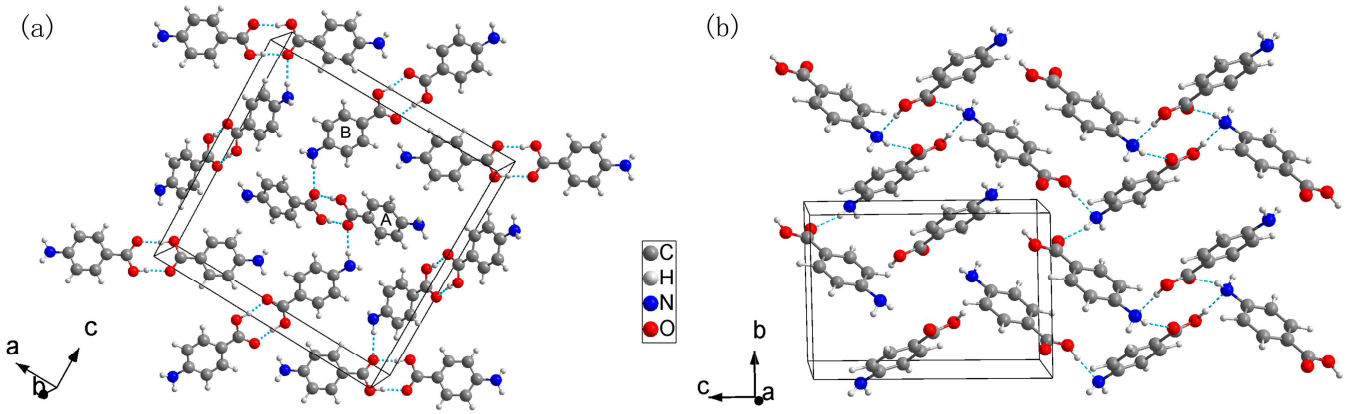

Fig. 1 Crystal structure of different polymorphs of *p*-aminobenzoic acid under ambient conditions: (a) α-PABA; (b) β-PABA; the hydrogen bonds are marked as dashed lines.

effects between hydrogen bonding and van der Waals interactions.

Results and discussion

Crystal structures at ambient conditions

Two crystalline forms of PABA can be obtained at ambient conditions. Figure 1 shows the molecular packing in both forms. The needle-shaped α-form crystals are acquired by evaporation from solvents, such as water, ethanol, acetone, acetic acid, and ethyl acetate.[28] This form is crystallized into the monoclinic $P2_1/n$ space group.[30] The unit cell dimensions are a = 18.55(1) Å, b = 3.86(0) Å, c = 18.64(2) Å, β = 93.56(0)° and V = 1332.32(0) Å^3. Eight and two molecules exist in the unit cell and the asymmetric unit. The dimensions of the two structurally distinct molecules (type A and B) are closely similar. The molecular pairs of each type are associated as dimers via two O–H···O bonds across a symmetry center. The O–H···O distances for pairs of A and B molecules are 2.64 and 2.61 Å; the respective O–H···O angles are 167° and 166°. The nitrogen atom of molecule B forms an N–H···O bond to molecule A (distance, 2.98 Å; angle, 174°). The β-form crystals exhibit prismatic shapes upon growth from water and ethyl acetate.[28] This form will be reproducibly crystallized at the cooling rate of 1 °C/min by controlled sonication.[31] The β-form crystallizes into the monoclinic $P2_1/n$ structure, with a = 6.27(8) Å, b = 8.58(3) Å, c = 12.36(4) Å, β = 100.13(3)° and V = 655.90(7) Å^3.[32] This form possess tetramer structures that involve four hydrogen bonds by alternating amino and carboxylic acid groups. The O–H···N and N–H···O distance are 2.75 and 3.04 Å; the respective angles are 160° and 164°.

Crystal structures and Raman spectra at high pressures

Assignments for the Raman modes of α-PABA are based on the reported literatures.[29, 33-35] Figure 2 illustrates the evolution of the Raman modes and the corresponding frequency shifts at 40−265 cm^{-1} and 3000−3420 cm^{-1} with various pressures. Ten external modes can be observed at 0.2 GPa (Figure 2(a)). The two modes marked by an asterisk overlap with increasing pressure and become too weak to be traced beyond 3.6 GPa. Another two modes with a rhombus cross each other because of different shift rates. All of the external modes exhibit blue shifts up to the highest pressure (Figure 2(b)). This shift is caused by the decrease in intermolecular distances and the increase in the strength of intermolecular interactions.[36-39] No abrupt changes in the external modes exist; the α-PABA is stable from 0 to 12.3 GPa.

Figure 2(c) summarizes three C−H and two N−H stretching vibrations; the former shifts toward higher frequencies. These C−H stretching modes lose their intensities and vanish into the scattering background above 10.2 GPa. In contrast to the other modes, obvious red shifts of the two N−H bands are observed below 5.2 GPa. The red shifts indicate that the hydrogen bonds in α-PABA are weak or moderately strong.[40-43] The distance between a nitrogen atom and a hydrogen atom shortens as the crystal is compressed, which agrees with the blue shifts of the external modes. The electrostatic attraction between H···O gets simultaneously enhanced; the N–H bond is extended. Furthermore, the strength of N–H···O hydrogen bonds constantly increases with increasing pressure. The two modes shift toward higher frequencies at different rates above 5.2 GPa; this shift suggests that N–H bonds participate in strong hydrogen bonds.[44]

Figure 3 shows the Raman patterns of α-PABA ranging from 600 cm^{-1} to 1710 cm^{-1}. The mode corresponding to the O=C−O out-of-plane bending evolves into the doublet bands at 2.7 GPa, which subsequently reduces the frequencies. A new peak (assigned as δ(C=O)) marked by an asterisk emerges and exhibits red shift from 2.7 GPa to 12.3 GPa. These behaviours are attributed to the local distortion of the bonds that connect carboxyl groups with aromatic ring. These C−C bonds can be easily distorted by the increasing external stress, because they are longer than the other bonds. At 5.2 GPa, the highest-frequency vibration band of the C−C bonds on aromatic rings splits into two (Figure 3(b)). Another band of this vibration (1603 cm^{-1}) loses its intensity at 8.3 GPa; the symmetry of the aromatic rings decreases progressively. All of the internal modes display blue shifts upon increasing pressure; these shifts arise from to the increased effective force constants with the contraction of interatomic distance.[45]

Raman modes of β-PABA are identified according to the literatures reported before.[29,33-35] Figure 4 reveals the representative high-pressure Raman patterns and the corresponding peak positions against the pressure at 50–260 cm^{-1} and 3020−3420 cm^{-1}. The mode marked with a dot loses its intensity at 0.4 GPa. Upon further compression, the Raman band with an asterisk evolves into the triplet bands at 1.2 GPa; the result is attributed to the different pressure-induced Raman shifts of the three adjacent modes at ambient pressure. The

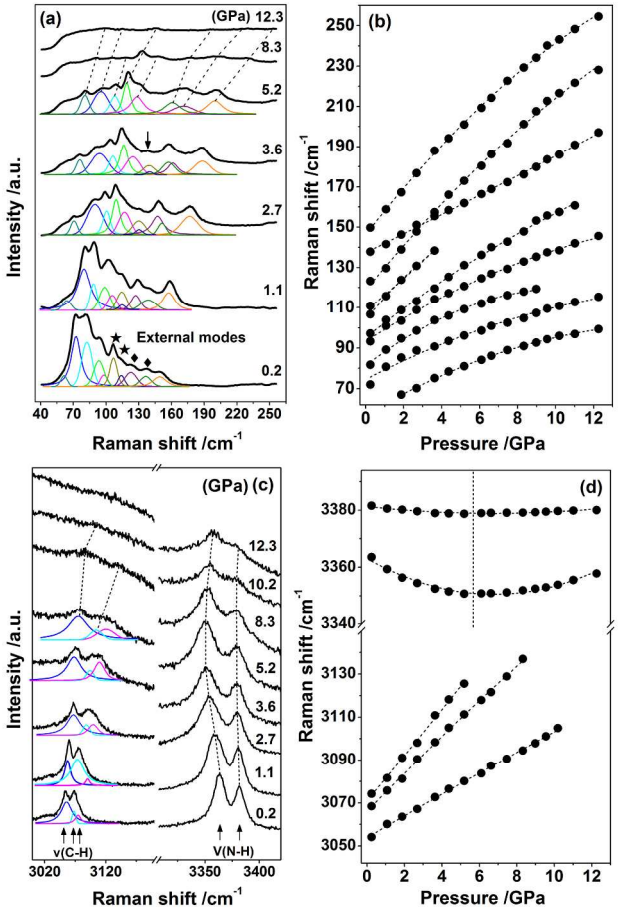

Fig. 2 Representive Raman spectra of α-PABA and the corresponding frequency shifts in the region of (a) 40−265 cm^{-1} and (b) 3000−3420 cm^{-1} at various pressures. Peak fitting and decomposition are obtained using a combination of Gaussian and Lorentzian functions. Frequency shifts are fitted to linear or quadratic function.

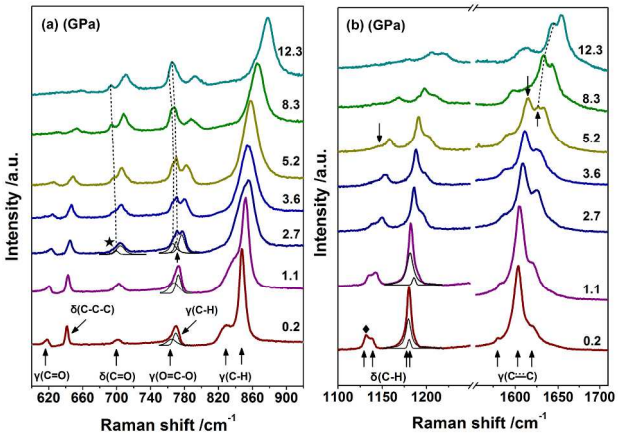

Fig. 3 Selected Raman spectra of α-PABA at various pressures in the ranges (a) 600−920 cm^{-1} and (b) 1100−1710 cm^{-1}. Decompositions of the spectra and the peak fits are illustrated for clarity. Dashed lines are used to indicate the modes' evolution.

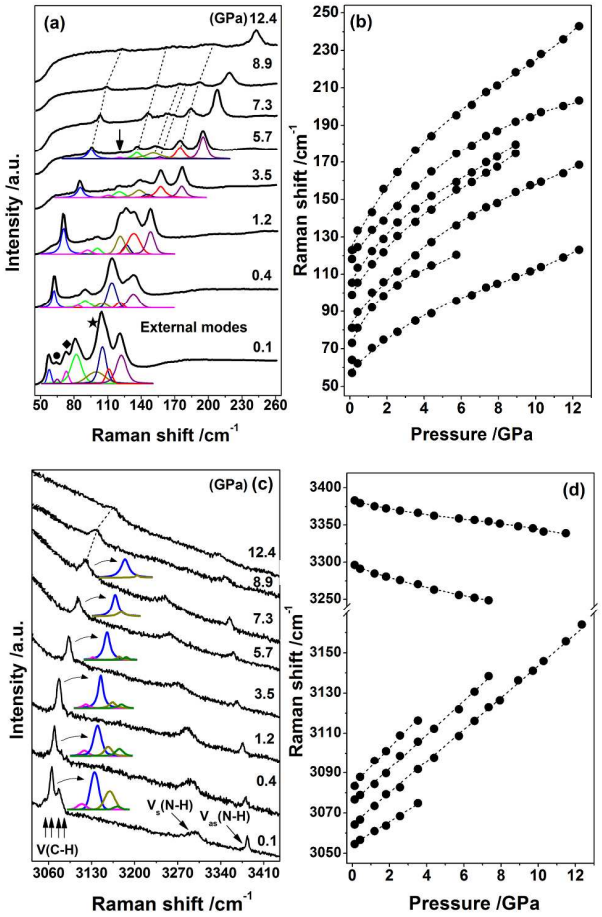

Fig. 4 Representive Raman spectra of β-PABA and the dependence of peak positions versus pressure in the region of (a) 50−260 cm^{-1} and (b) 3020−3420 cm^{-1}. Peak fitting and decomposition are obtained using mixed Gaussian/Lorentzian curves. Shifts of these modes are fitted to linear or quadratic function.

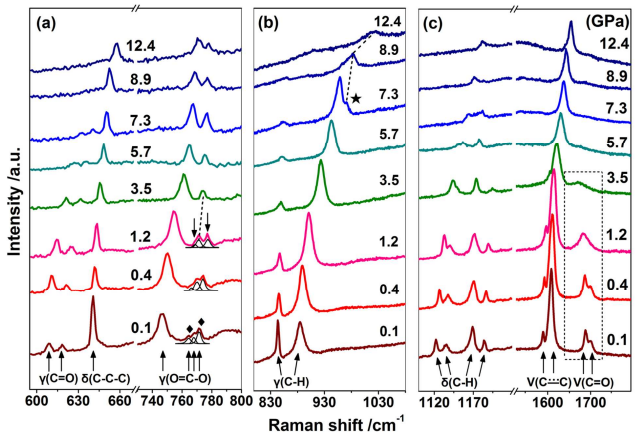

Fig. 5 Selected Raman spectra of the internal modes of β-PABA in the range of 580−1800 cm^{-1}. Peak fitting and decomposition are shown for clarity. Dashed lines are conducted for the evolution of the modes.

modes with a rhombus are too weak to be followed above 5.7 GPa. All of the external modes gradually shift toward higher frequencies without any discontinuity; no phase transition is observed up to 12.4 GPa.

Figure 4(c) shows the observed C−H and N−H stretching regions. The spectrum of the C−H stretching vibrations comprises four bands at 0.1 GPa; these bands exhibit continuous blue shifts. According to the assignment, the band (3297 cm^{-1}) is identified as symmetric N−H stretching vibration; reversely, 3383 cm^{-1} corresponds to the asymmetric stretching vibration. The frequencies of the two N−H modes decrease with increasing pressure. The result can be elucidated

by considering the weak or moderately strong N–H···O hydrogen bonds in β-PABA.[40-43]

Figure 5 shows the Raman spectra of β-PABA ranging from 580 cm^{-1} to 1800 cm^{-1}. The two bands marked by a rhombus, denoted as the O=C–O out-of-plane bending vibration, absolutely lose their intensities at 3.5 GPa. The γ (O=C–O) in β-PABA do not display red shifts as in α-PABA, because of different environments from molecular arrangements. Further compression to 7.3 GPa forms a new band with an asterisk at 969 cm^{-1}, indicative of the distortions of the C–H bonds. A red shift for the C=O stretching mode disappears at 5.7 GPa; this shift is caused by the pressure-induced enhancement of the N–H···O=C hydrogen bonds. The pressure reduces the interatomic distances; the electrostatic attraction between H and O increases, which results in the extension of the C=O distance.

Overall, there is no evidence of a new polymorph or a transformation between the two polymorphs, as under high temperatures. The temperature increases the bond distances and atomic mobilities, whereas the pressure has the opposite influence.[46] Accordingly, pressure and temperature yield different effects on the structural stability of *p*-aminobenzoic acid polymorphs.

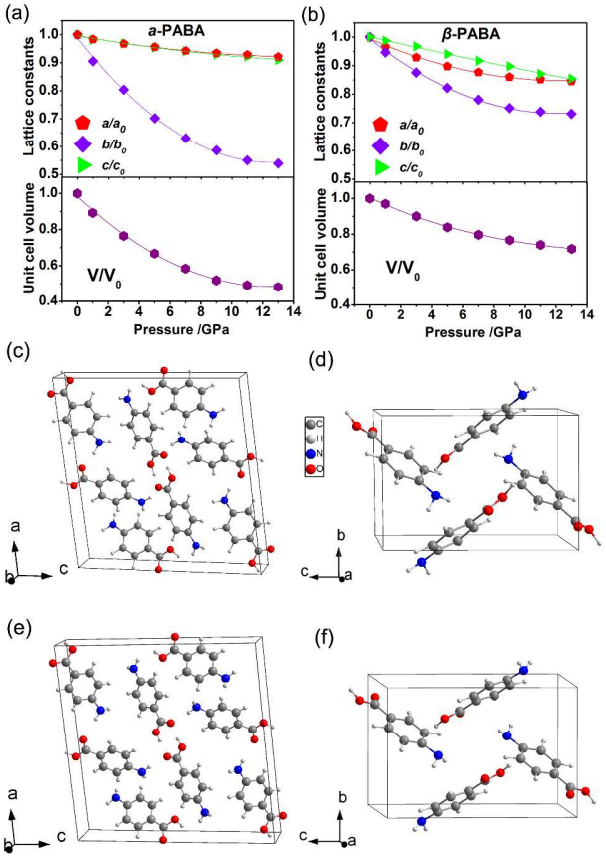

Fig. 6 Calculated lattice constants and unit cell volume (a) (b); unit cells of α-PABA (c) and β-PABA (d) at 13 GPa; unit cells of α-PABA (e) and β-PABA (f) at ambient pressure.

Hydrogen bonds under high pressures have practical significance for physics, chemistry, and life sciences. The changes in hydrogen bonds can be obtained by *ab initio* calculations, because the α- and β-PABA remain their structural stabilities under high pressures. Figure 6 depicts the pressure dependences of the unit cell parameters as well as the crystal structures at 13 GPa. The molecules undergo rotations, distortions, and close packing at certain degrees under high pressures. Furthermore, the compressional behaviours of the two unit cells are markedly different. α-PABA presents much more noticeable anisotropic characteristics than β-PABA. The most compressible parameter in α-form crystal is the *b*-axis; the largest change of 46.053(26)% occurs at 13 GPa. The relative compressions of *a*- and *c*-axes are 7.897(68)% and 8.968(69)%, respectively. In β-form crystal, the relative reduction of *b*-axis is 26.936(44)%; the *a*- and *c*-axis are compressed by 14.537(37)% and 14.529(27)%. This fact leads to the molecular planes (parallel to 011 and 0-11) rotating and contracting faster than the other intermolecular distances. Changes in the monoclinic β angles are dissimilar; this angle decreases by 7.897(68)% in α-PABA, but changes by -0.294(73)% in β-PABA. The anisotropic compressional behaviours of the two polymorphs are attributed to the hydrogen-bonded networks. The direction of *a*-axis in α-PABA is mostly parallel to the O–H···O hydrogen bonds of type *A* molecules; the *c*-axis coincides with the directions of O–H···O hydrogen bonds of type *B* molecules. The *b*-axis, however, is almost perpendicular to all the types of hydrogen bonds. The hydrogen bonding can effectively prevent close packing along its direction; the compressional behaviour of α-PABA is anisotropic. For the same reason, the *a*- and *c*-axes are respectively close to the N–H···O and O–H···N hydrogen bonds in β-PABA; the *b*-axis does not correspond to the direction of any hydrogen bonds.

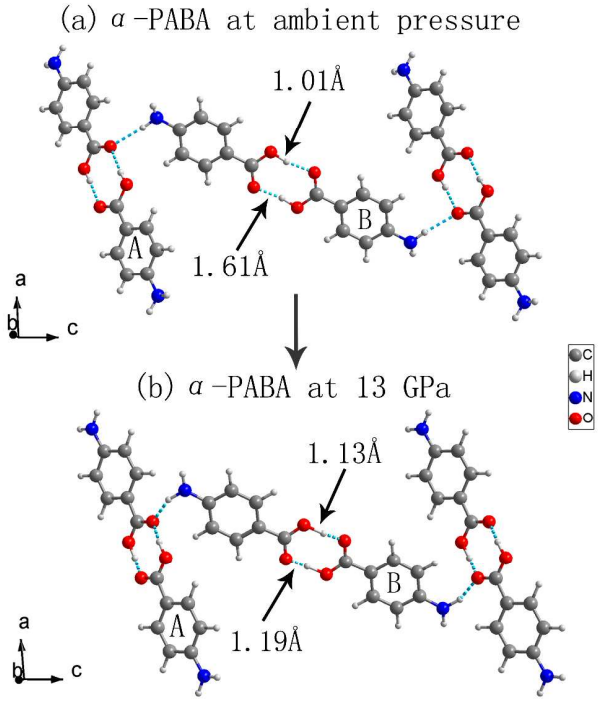

Fig. 7 The symmetrization of the O–H···O hydrogen bonds of type *B* molecules of α-PABA at 13 GPa and the dimer polymerization.

Table 1 tabulates the calculated changes in the D···A, D–H, and H···A distances (D and A mean donor and acceptor, respectively). The D···A and H···A distances in α- and β-form crystals reduce with increasing pressure; the hydrogen bonds strength are enhanced. The O–H distance increases in both forms; while the corresponding stretching vibrations appear in calculations, these vibrations are too weak to be observed in experiments. The O–H distance increases to 1.13 Å and the H···O distance decrease to 1.19 Å for pairs of type *B* molecules,

Pressure (GPa)	O−H···O (*α-A*)		O−H···O (*α-B*)		N−H···O (*α*)		O−H···N (*β*)		N−H···O (*β*)	
	Δr (O−H)	Δr (H···O)	Δr (O−H)	Δr (H···O)	Δr (N−H)	Δr (H···O)	Δr (O−H)	Δr (H···N)	Δr (N−H)	Δr (H···O)
1	0.004	-0.027	0.02	-0.056	0.002	-0.103	0.008	-0.066	0.001	-0.051
3	0.013	-0.064	0.037	-0.106	0.004	-0.222	0.016	-0.128	0.002	-0.083
5	0.022	-0.101	0.057	-0.152	0.005	-0.338	0.024	-0.181	0.003	-0.102
7	0.023	-0.115	0.064	-0.18	0.005	-0.401	0.033	-0.227	0.006	-0.119
9	0.025	-0.128	0.072	-0.206	0.004	-0.442	0.041	-0.262	0.007	-0.125
11	0.029	-0.147	0.074	-0.216	0.003	-0.472	0.055	-0.307	0.009	-0.134
13	0.032	-0.156	0.077	-0.221	0.002	-0.492	0.061	-0.327	0.013	-0.141

Table 1 *Ab initio* calculated pressure-induced changes in bond lengths (Å) for hydrogen bonds of *α*-PABA and *β*-PABA; positive and negative values indicate elongation and shortening, respectively.

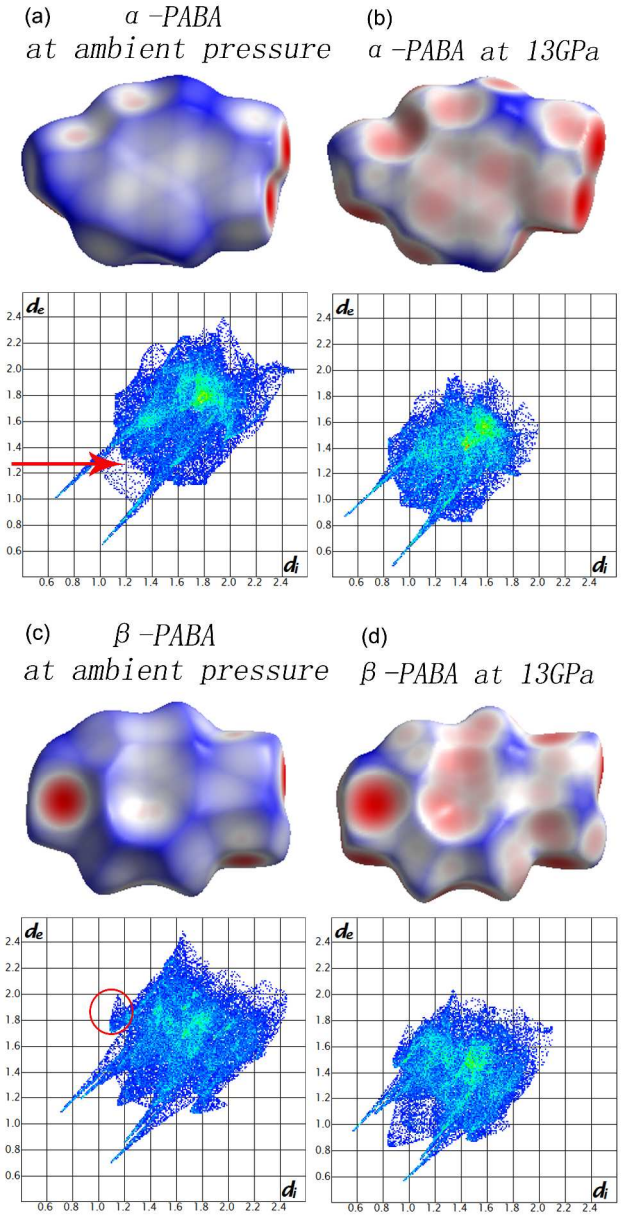

Fig. 8 Hirshfeld surfaces mapped with dnorm and fingerprint plots for *α*-PABA and *β*-PABA at ambient pressure and 13 GPa.

implying the symmetrisation of the O−H···O hydrogen bonds at 13 GPa (Figure 7). This indicates that the electron cloud of H atom is almost equally distributed between the two O atoms; the hydrogen bonds possess a substantial covalent characteristic. Van der Waals repulsion, electrostatic, and covalent interactions are the three major contributions to the energies of O−H···O hydrogen bonds. Lippincott[47] found that the electrostatic contribution is submerged by increase in covalent contribution for close distances of approach. In most systems with hydrogen bonds and carboxylic acid dimers, the dissociation energy of these systems may exhibit a low and thermally surmountable barrier; the O−H···O hydrogen bonds have an approximate covalent contribution when positioned close enough.

For type *A* molecules, however, the O atoms also act as acceptors of the N−H···O hydrogen bonds; the atoms counteract partial attractive interaction from the H atoms of O−H···O, so that the *A* molecules do not undergo polymerization process. Comparing with the continuous extended N−H bonds in *β*-PABA, the N−H distance in *α*-PABA first increases and then decreases, which well agree with our Raman results. This can be explained by the different constructed hydrogen bonds of both forms. The ability of the amino nitrogen to accept hydrogen bonds decreases, because the carboxylic acid groups pull the electrons from nitrogen atom through the π system of the aromatic ring.[48] Nitrogen and hydrogen both show positive electricity; the interactions between these positively charged centers are repulsive. When an amino nitrogen serves as hydrogen-bond acceptor, this atom will possess a high sensitivity to the decrease of the distance.[49] The enhanced repulsive interaction will cause the torsions of the four-membered hydrogen-bonded networks with increasing pressure; the impact on the N−H bonds is reduced. The free N−H bonds of both forms reveal the same tendency as those participating in the hydrogen bonds. This is attributed to the attractive interaction between the positive hydrogen atoms and other electron-rich atoms around H.

Hirshfeld surface and fingerprint plot allow the intermolecular interactions the direct comparison to identify the changes in packing patterns (Figure 8).[50] Increasing pressure produces more red regions on the Hirshfeld surface; close intermolecular interactions significantly increase. Overall, the fingerprint plot moves towards the origin upon shortening of the contacts. The blue-green area centred at (1.9, 1.9) results from the stacking between the benzene rings of one dimer and the carboxylate group of another dimer. In the fingerprint plot of *α*-PABA at ambient pressure, the "skirt" points (de≈di at

around the van der Waals radius of the H-atom of 1.2 Å) with a red arrow derived from short H···H contacts of approximately 2.4 Å; the plot reveals the characteristic of a cyclic hydrogen-bonded dimer. The contribution of the H···H interaction shows small changes from 41.6% at ambient pressure to 39.9% at 13 GPa. The H···H contacts are compressed to 1.9 Å; no phase transition occurs. Two prominent "spikes" are characteristic of the formation of O–H···O and N–H···O bonds. The upper spike corresponds to the hydrogen-bond donor, whereas the lower spike corresponds to the hydrogen-bond acceptor. The contribution of the H···O contacts also undergoes small changes from 25.9% at ambient and 24.4% at 13 GPa. The fingerprint plot of β-PABA exhibits significant differences from α-PABA, although the two forms have the same molecular type. In β-PABA, the "wings" areas are related to C–H···π interaction with the contribution unchanged at 25.1%. The points related to H···H contacts reveal the patterns arising from two different contacts; the chemical environment of the two regions is somewhat different. Moreover, the distance of H···H contacts is compressed from 2.4 Å to 2.0 Å, and the contributions are reduced from 36.4% at ambient pressure to 33.6% at 13 GPa. β-PABA reveals two pairs of hydrogen-bond spikes; the longer of which corresponds to the closer O–H···N hydrogen bond, and the shorter of which corresponds to the more distant N–H···O hydrogen bond. The contributions of the two hydrogen bonds are reduced by 0.5% and 0.4%, respectively.

Hydrogen bonding and van der Waals interactions are the predominant cohesive factors for the crystal arrangements of α- and β-PABA at ambient pressure. The structural stability is attributed to the unique dimer and tetramer structures as well as the cooperative nature of the two interactions. As a function of external pressure, the molecules in the crystals become closer to each other to achieve closer packing; the hydrogen bonding and van der Waals interactions increase. For α-PABA, however, the molecular pairs are connected via two O–H···O bonds; a hydrogen-bonded bridge is formed between the two molecules. This bridge resists the effect of pressure along the direction of hydrogen bonds. This visualization is analogous to the behaviours of α- and δ- forms in pyrazinamide (PZA) polymorphs.[51] For the tetramer structure of β-PABA, the special four-membered hydrogen-bonded networks can easily twist to release the increased intermolecular interactions, as well as maintain the balance of hydrogen bonding and van der Waals interactions; the structural stability is maintained.

Experimental Section

Sample and high-pressure technique details.

The commercially available α-PABA, purchased from Alfa Aesar with a purity of 99%, was used as the source material. Two pure forms (α and β) of PABA were synthesized in terms of the procedures reported previously.[28] The original material was dissolved into deionized water to form a saturated solution at about 20 °C. This solution was left evaporating and undisturbed for a couple of weeks at this temperature. The rate of evaporation was adjusted by covering with plastic film with a few small holes. Crystals with two different morphologies, needles for the α form and prisms for the β form, were collected respectively after the solution evaporated completely. The identity and crystallinity of the two crystals were confirmed by Raman spectra.

The symmetric diamond anvil cell (DAC) was used to perform all the high-pressure Raman scattering measurements. The cell consists of two culet diamonds with a face of 400 μm in diameter. T301 steel gaskets were preindented to a thickness of 50 μm, and center holes with a diameter of 130 μm were drilled as the sample chamber. Single-crystal samples together with one or two ruby balls were loaded into the hole. The well-established ruby luminescence technique was applied to do the pressure calibration. The pressure conditions were determined on the basis of R1 line shift with an accuracy of 0.1 GPa throughout the whole experiments. Due to the dissolution in ethanol, we choose silicone oil as pressure transmitting medium.

High-pressure Raman spectroscopy.

Raman measurements were conducted with the Acton SpectraPro 2500i spectrometer equipped with a liquid nitrogen cooled CCD camera (Pylon: 100B). The 532 nm line of diode laser was employed to excite the sample. The output power of the laser was set to 10 mW on the sample, and the accumulation time for each spectrum is 30 s. The spectral resolution was approximately 1 cm−1. For all experiments at each pressure, the DAC was maintained for ~5 minutes to stabilize the pressure in the sample chamber. All experiments were performed at room temperature. All selected Raman bands were fitted when necessary using a combination of Gaussian and Lorentzian functions.

***Ab initio* calculations.**

Further analysis was performed by employing the program Materials Studio 5.0. Our simulations at 0 K and equivalent hydrostatic pressure were carried out based on the structures reported before.[30,32] The norm-conserving pseudopotential plane-wave method with reciprocal space as representation implemented in the CASTEP code had been used. The exchange-correlation effects were treated within the generalized gradient approximation (GGA) of PW91. The geometry optimizations in this paper including the lattice constants and the unit cell volumes were performed by the BFGS algorithm. Convergence tests gave 830 eV kinetic energy cutoff and 45×54×80 FFT grid density with 1.0 scaling factor. We used smart apply finite basis set correction with automatic correction mode and 3 points numerical differentiation. The k-point was of fine quality with 0.05 $Å^{-1}$ separation.

Conclusions

In summary, we investigate the two forms (α, β) of *p*-aminobenzoic acids (PABA) under high pressures through the evolutions of the Raman spectra and *ab initio* calculations. Experimental and calculated results suggest that both forms are stable up to ~13 GPa. The high-pressure behaviours of the two polymorphs are systematically compared. We propose the stability is attributed to the crystal structures and hydrogen bonding interaction. High-pressure investigations of hydrogen-bonded polymorphs can provide insight into the nature of structure−property relationships, which are conducive to design crystals with predefined and desired architectures by means of hydrogen-bonded networks in crystal engineering.

Acknowledgements

This work is supported by NSFC (Nos. 91227202, 21073071, and 11204101), RFDP (No. 20120061130006), National Basic Research Program of China (No. 2011CB808200), China Postdoctoral Science Foundation (NO. 2012M511327).

Notes and references

[a] State Key Laboratory of Superhard Materials, Jilin University, Changchun 130012, China.
E-mail: zoubo@jlu.edu.cn

Electronic Supplementary Information (ESI) available: *Ab initio* calculated unit-cell parameters and atomic coordinates of α-PABA and β-PABA at 0 GPa, 7 GPa, and 13 GPa, respectively. See DOI: 10.1039/b000000x/

1 W. C. McCrone, D. Fox, M. M. Labes and A. Weissberger, *Physics and Chemistry of the Organic Solid State*. 1965, 725.
2 D. Braga, L. Maini, C. Fagnano, P. Taddei, M. R. Chierotti and R. Gobetto, *Chem-Eur. J.* 2007, **13**, 1222.
3 S. Jiang, J. H. ter Horst and P. J. Jansens, *Cryst. Growth Des*. 2007, **8**, 37.
4 W. David, K. Shankland, C. Pulham, N. Blagden, R. Davey and M. Song, *Angew. Chem. Int. Ed*. 2005, **44**, 7032.
5 A. Gavezzotti and G. Filippini, *J. Am. Chem. Soc*. 1995, **117**, 12299.
6 A. Nangia *Acc. Chem. Res*. 2008, **41**, 595.
7 J. Bernstein, *Polymorphism in molecular crystals*; Oxford University Press, 2002; Vol. **14**.
8 W. W. Porter Iii, S. C. Elie and A. J. Matzger, *Cryst. Growth Des*. 2008, **8**, 14.
9 E. Nauha, H. Saxell, M. Nissinen, E. Kolehmainen, A. Schäfer and R. Schlecker, *CrystEngComm* 2009, **11**, 2536.
10 A. D. Bond, R. Boese and G. R. Desiraju, *Angew. Chem. Int. Ed.* 2007, **46**, 615.
11 E. H. Lee, S. X. Boerrigter, A. C. Rumondor, S. P. Chamarthy and S. R. Byrn, *Cryst. Growth Des*. 2008, **8**, 91.
12 K. Wang, D. F. Duan, M. Zhou, S. R. Li, T. Cui, B. B. Liu, J. Liu, B. Zou and G. T. Zou, *J. Phys. Chem. B* 2011, **115**, 4639.
13 K. Wang, D. F. Duan, R. Wang, A. L. Lin, Q. Cui, B. B. Liu, T. Cui, B. Zou, X. Zhang and J. Z. Hu, *Langmuir* 2009, **25**, 4787.
14 T. T. Yan, S. R. Li, K. Wang, X. Tan, Z. M. Jiang, K. Yang, B. B. Liu, G. T. Zou and B. Zou *J. Phys. Chem. B* 2012, **116**, 9796.
15 K. Wang, D. F. Duan, R. Wang, D. Liu, L. Y. Tang, T. Cui, B. B. Liu, Q. Cui, J. Liu and B. Zou, *J. Phys. Chem. B* 2009, **113**, 14719.
16 S. A. Moggach, D. R. Allan, C. A. Morrison, S. Parsons and L. Sawyer, *Acta Crystallogr. B* 2005, **61**, 58.
17 E. Boldyreva, T. Shakhtshneider, H. Ahsbahs, H. Sowa and H. Uchtmann, *J. Therm. Anal. Calorim*. 2002, **68**, 437.
18 A. Dawson, D. R. Allan, S. A. Belmonte, S. J. Clark, W. I. David, P. A. McGregor, S. Parsons, C. R. Pulham and L. Sawyer, *Crystal Growth & Design* 2005, **5**, 1415.
19 D. M. Martins, C. K. Spanswick, D. S. Middlemiss, N. Abbas, C. R. Pulham and C. A. Morrison, *J. Phys. Chem. A* 2009, **113**, 5998.
20 L. B. Munday,P. W. Chung,B. M. RiceandS. D. Solares The Journal of Physical Chemistry B 2011, **115**, 4378.
21 I. D. Oswald, and A. J. Urquhart, *CrystEngComm* 2011, **13**, 4503.
22 V. S. Minkov, S. V. Goryainov, E. V. Boldyreva and C. H. Görbitz, *J. Raman Spectrosc.* 2010, **41**, 1748.
23 F. P. A. Fabbiani, D. R. Allan, S. Parsons and C. R. Pulham, *CrystEngComm* 2005, **7**, 179.
24 R. Killean, P. Tollin, D. Watson and D. Young, Acta Crystallogr. 1965, **19**, 482.
25 M. Kuhnert-Brandstaetter and H. Grimm, *Mikrochim, Acta* 1969, **6**, 1208.
26 O. Jarchow, *Neues Jahrb. Mineral., Abh*. 1968, **109**, 211.
27 A. Banerjee, P. Agrawal and R. C. Gupta, *J. Prakt. Chem.* 1973, **315**, 251.
28 S. Gracin and Å. C. Rasmuson, *Cryst. Growth Des*. 2004, **4**, 1013.
29 X. Yang, X. Wang and C. B. Ching, *J. Raman Spectrosc* 2009, **40**, 870.
30 T. Lai and R. E. Marsh, *Acta Crystallogr* 1967, **22**, 885.
31 S. Gracin, M. Uusi-Penttilä and Å. C. Rasmuson, *Cryst. Growth Des* 2005, **5**, 1787.
32 S. Gracin and A. Fischer, *Acta Crystallogr. E* 2005, **61**, o1242.
33 M. Samsonowicz, T. Hrynaszkiewicz, R. Świsłocka, E. Regulska and W. Lewandowski, *J. Mol. Struct*. 2005, **744**, 345.
34 R. Świsłocka, M. Samsonowicz, E. Regulska and W. Lewandowski, *J. Mol. Struct*. 2006, **792**, 227.
35 N. Sundaraganesan, S. Ilakiamani and B. Dominic Joshua, *Spectrochim. Acta, Part A* 2007, **67**, 287.
36 J. A. Ciezak, T. A. Jenkins, Z. Liu and R. J. Hemley, *J. Phys. Chem. A* 2007, **111**, 59.
37 T.-R. Park, Z. A. Dreger and Y. M. Gupta, *J. Phys. Chem. B* 2004, **108**, 3174.
38 R. Rao, T. Sakuntala and B. Godwal, *Phys. Rev. B* 2002, **65**, 054108.
39 A. F. Goncharov, M. R. Manaa, J. M. Zaug, R. H. Gee, L. E. Fried and W. B. Montgomery, *Phys. Rev. Lett*. 2005, **94**, 065505.
40 M. Pravica, B. Yulga, Z. Liu and O. Tschauner *Phys. Rev. B* 2007, **76**, 064102.
41 S. Hamann and M. Linton, *Aust. J. Chem*. 1975, **28**, 2567.
42 S. Moon and H. Drickamer, *J. Chem. Phys.* 1974, **61**, 48.
43 J. R. FSC and S. S. Sternstein, *J. Chem. Phys.* 1964, **41**, 47.
44 R. Custelcean and Z. A. Dreger, *J. Phys. Chem. B* 2003, **107**, 9231.
45 I. Orgzall, O. Franco and B. Schulz, J. Phys.: Condens. Matter 2006, 18, 5269.
46 J. L. Jordá, F. Rey, G. Sastre, S. Valencia, M. Palomino, A. Corma, A. Segura, D. Errandonea, R. Lacomba and F. J. Manjón, *Angew. Chem*. 2013, **40**, 10652.
47 E. R. Lippincott, *J. Chem. Phys.* 1955, **23**, 603.
48 S. Gracin, T. Brinck and Å. C. Rasmuson, *Ind.Eng. Chem. Res*. 2002, **41**, 5114.
49 Z. Nahosse, L. Christian and L. Q. Jean-Yves, *CrystEngComm* 2002, **4**, 326.
50 P. A. Wood, J. J. McKinnon, S. Parsons, E. Pidcock and M. A. Spackman, *CrystEngComm* 2008, **10**, 368.
51 X. Tan, K. Wang, S. R. Li, H. S. Yuan, T. T. Yan, J. Liu, K. Yang, B. B. Liu, G. T. Zou and B. Zou, *J. Phys. Chem. B* 2012, **116**, 14441.